Bulgarian Chemical Communications, Volume 53, Special Issue A (pp. 080 – 084) 2021 DOI: 10.34049/bcc.53.A.0010

Silica supported iron and chromium oxide catalysts for methanol decomposition

G. Issa*[1], N. Velinov[2], D. Kovacheva[2], T. Tsoncheva[1]

[1] *Institute of Organic Chemistry with Centre of Phytochemistry, Bulgarian Academy of Sciences, Acad. G. Bonchev Str. Bl. 9, 1113 Sofia, Bulgaria*

[2] *Institute of General and Inorganic Chemistry, Bulgarian Academy of Sciences, Acad. G. Bonchev Str. Bl. 11, 1113 Sofia, Bulgaria*

Received January 31, 2021; Revised March 25, 2021

In present study mesoporous iron–chromium oxide silica materials with different composition were prepared by wet impregnation method. The obtained composites were characterized by XRD, UV-Vis, FTIR, Mossbauer spectroscopy and temperature programmed reduction (TPR). The catalytic behaviour of the samples was tested in methanol decomposition to syngas. The effect of phase composition on the structure and redox properties was discussed in close relation with their catalytic activity and CO selectivity. It was found that the catalytic behavior of the samples in the methanol decomposition could be successfully controlled by the Fe/Cr ratio.

Key words: iron and chromium oxide catalysts; methanol decomposition

INTRODUCTION

Methanol is expected to become one of the new liquid energy carriers because it can be synthesized from biomass, coal and natural gas, all of them being more abundant resources than the crude oil. In the last two decades among the various procedures of methanol conversion (steam reforming, partial oxidation, etc.), methanol decomposition has received growing attention as a source of hydrogen and synthesis gas for chemical reactions or as an ecological fuel for gas turbines, vehicles and fuel cells [1-6]. The synthesis and characterization of novel multicomponent nanosized materials have been intensively investigated because of their wide application in various fields, in particular in the field of catalysis [7-10]. The requirements for them are high, both for their activity, selectivity and stability during operation, as well as from an economic point of view - low cost and ability to operate at relatively low temperatures. These issues are in the focus of many studies and patents in which innovative porous materials based on transition metals and nanosized metal oxides are used [11, 12]. They are one of the most important and widely used categories of solid catalysts that could be used both as active phases and supports. They have been widely used for various catalytic reactions, including oxidation, dehydration, dehydrogenation and isomerization [10-12]. The mixed metal oxides are oxygen-containing combinations of two or more metal ions, which ratio can be varied or defined by strict stoichiometry. Furthermore, the nanosized materials consisting of more components in different proportions reveal unlimited possibilities to improve the catalytic properties of materials through structural, phase composition and textural changes, improved thermal stability, changes in the acid-basic and redox properties and the occurrence of synergistic effects between the individual components. Large scale application of iron oxide with small particles and tailoring of specific properties have prompted the development of widely used chemical methods, including sol–gel methods, microwave plasma, host template, co-precipitation, micro emission methods, citrate precursor techniques and mechanical alloying for the fabrication of stoichiometric and chemically pure spinel ferrite nanoparticles [13-15]. Iron–chromium oxides, both in crystalline and amorphous states, were obtained using ultrasonic radiation hydrothermal methods, and thermal decomposition of mixtures of salts as metal sources [16-20]. The Fe_2O_3–Cr_2O_3 mixed oxide system has been widely studied due to its potential application as catalysts in wide range of reactions especially in the high temperature water gas shift reaction, dehydration of ethyl benzene to styrene, oxidative dehydrogenation of butene to butadiene, etc [16-18]. The magnetite (Fe_3O_4) type of iron oxide was found to be the active phase of WGS reaction [21]. It was found the role of chromium is believed to increase the surface area of catalyst and prevent sintering, thus increasing catalyst life time. It is also

* To whom all correspondence should be sent:
E-mail: *issa@abv.bg*

reported by Instituto *et al.* [22], copper improves the performance of the iron and chromium based catalysts towards the high temperature shift reaction, by increasing the intrinsic activity. Nair and Kurian [23] tested chromium substituted zinc ferrite nanocatalysts for the degradation of 4-chlorophenol, 2,4-dichlorophenol and 2,4-dichlorophenoxy acetic acid by wet peroxide oxidation process. It is established that chromium substitution increased the activity of zinc ferrite catalyst and the unsubstituted chromium ferrite exhibited highest activity. Moreover, Gonzalez *et al.* [24] study the reduction properties of high temperature water gas shift catalysts (Cr_2O_3 added to Fe_2O_3) with various of reducing mixture. In their study, chromium is believed to act as a dispersing agent which makes Fe_2O_3 reduction process become easier. This study is focused on the preparation and characterization of series of supported on silica iron-chromium mixed oxides by wet impregnation techniques. Their application as catalysts for methanol decomposition was studied in details. The elucidation of the relation between the Fe/Cr ratio and the structure, texture, morphology, surface and catalytic properties of the obtained materials was the main challenge in the study. For the purpose, the obtained materials were characterized by a complex of different physicochemical techniques, such as XRD, FTIR, UV-Vis and Mossbauer spectroscopies and TPR with hydrogen.

EXPERIMENTAL

Iron and chromium supported on silica (Cabosil M5, 99.8%) materials with total metal content of 6 wt.% were prepared by wet impregnation method of silica with $Fe(NO_3)_3.9H_2O$ (≥98%) and/or $Cr(NO_3)_3.9H_2O$ (99%) aqueous solution in appropriate ratio. The powder samples were calcined at 773 K for 2 h in nitrogen atmosphere and denoted as $mFenCr/SiO_2$ where m/n corresponds to the ratio between the amount of different metals in wt.%

Powder X-ray diffraction study was performed on a Bruker D8 Advance diffractometer with Cu Kα radiation (λ=1.5406 Å) and a LynxEye detector with constant step of 0.02° 2θ and counting time of 17.5 s per step. The FTIR and UV-Vis spectra were recorded on a Bruker Vector 22 FTIR spectrometer and Jasco V-650 apparatus, respectively. The Mossbauer spectra were obtained on a with a Wissel (Wissenschaftliche Elektronik GmbH, Germany) electromechanical spectrometer using 57Co/Rh source and α-Fe standard. The TPR/TG (temperature-programmed reduction/ thermo-gravimetric) analyses were performed in a DSC/TGA NETZSCH instrument. Typically, 20 mg of the sample were placed in a microbalance crucible and heated in a flow of 50 vol.% H_2 in Ar (100° cm^3 min^{-1}) up to 773 K at 5 $K.min^{-1}$ and a final hold-up of 1 h. Methanol conversion was carried out in a fixed bed flow reactor (0.055 g of catalyst), argon being used as a carrier gas (50 $cm^3.min^{-1}$). The methanol partial pressure was 1.57 kPa. The catalysts were tested under conditions of a temperature-programmed regime within the range of 350–770 K with heating rate of 1 $K.min^{-1}$. On-line gas chromatographic analyses were performed on SCION INSTRUMENTS equipped with flame ionization and thermo-conductivity detectors, on a PLOT Q column, using an absolute calibration method and a carbon based material balance.

RESULTS AND DISCUSSION

Fig. 1 shows X-ray diffraction (XRD) patterns of the iron and chromium supported on silica materials. In case of the iron modification, the slight reflections at 35.4º, 42.8º, 56.7 º and 62.6º 2θ are detected [19]. They could be indexed to (311), (400) (511) and (440) planes of cubic Fe_3O_4 with crystallite size of about 10 nm. The patterns of chromium modification exhibit reflections at 33.6º, 43.5º and 64.3º 2θ which are assigned as Cr_2O_3 with average crystallite size of about 9 nm [20].

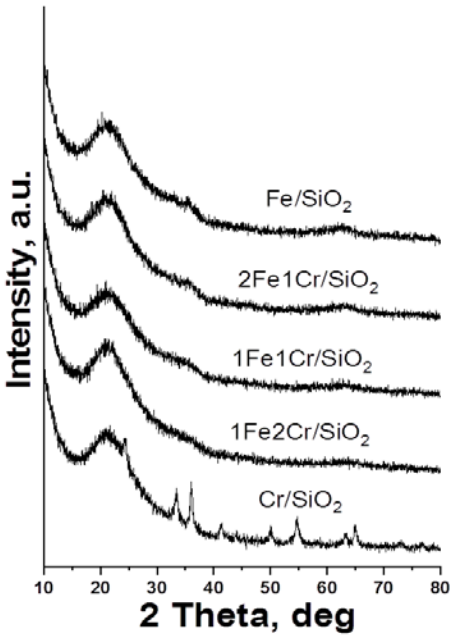

Fig. 1. XRD patterns of all iron and chromium oxide materials.

The XRD patterns of all mixed oxide (Fig. 1) represent very broad peaks and no reflections associated with the iron and chromium oxides are observed, probably due to their high dispersion. The formation of $Cr_{1.5}Fe_{1.5}O_4$ and $CrFe_2O_4$ mixed oxide with spinel structure has been reported [19, 22-25]. Similar tendency for homogeneous spreading of Cr^{3+} ions in the magnetite lattice by occupying of the octahedral sites and a simultaneous transfer of the displaced Fe^{2+} and Fe^{3+} ions to tetrahedral sites was reported in [25].

FTIR spectra of all silica materials consist of intense bands at around 1080, 800 and 450 cm^{-1}, which are typical of the characteristic symmetric and asymmetric vibrations of Si-O-Si bridges in silicas (Fig. 2a) [12]. The band around 1600 cm^{-1} is due to the adsorbed water molecules and the broad band in the interval 3100–3700 cm^{-1} is assigned to O-H stretching vibrations. The band at 538 cm^3 is assigned to Cr-O vibration, whereas a wider band centered at 640 cm^3 could be assigned to Fe-O vibrations [26-28]. The band around 960 cm^{-1} is more complicated and it is assigned generally to Si-O stretching vibrations in defect Si-O-M structures, where M is metal ion (Fig. 2a) [29]. The slight shift of the band as compared to pure silica support [29] indicates interaction between metal oxide species and surface silanol groups. This interaction seems to decrease for bi-component iron-chromium materials, probably due to the creation of new contact between both metal oxide nanoparticles.

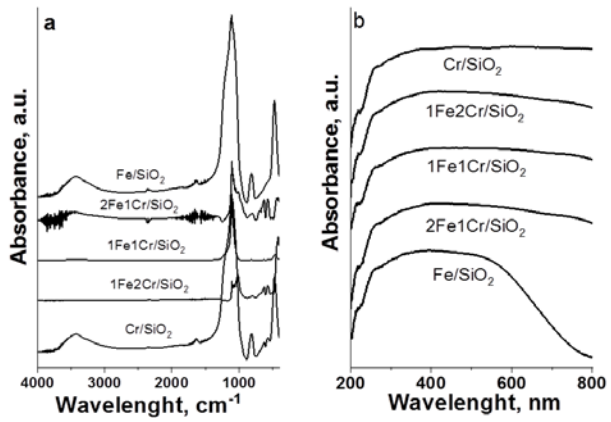

Fig. 2. FTIR spectra (a) and UV-Vis spectra (b) for all iron and chromium oxide materials.

The UV-Vis spectrum of pure iron oxide represents a broad absorption band in the 240-400 nm region which could be due to the superposition of various features assigned to mononuclear Fe^{3+} ions in octahedral coordination, small $(FeO)_n$ clusters and/or Fe_2O_3 particles (Fig. 2b) [30-32]. The small absorption band observed below 250 nm is possibly related to the presence of Fe^{3+} cations in tetrahedral coordination (Fig. 2b). The bands with maxima at about 250–300 and 300–400 nm can be connected with the presence of monomeric iron cations in octahedral coordination, while the band located above 400 nm is related to Fe_2O_3 particles [30]. The observed blue shift of these peaks for Fe/SiO_2 in comparison with bi-component oxides indicates the higher dispersion of iron nanoparticles in mixed materials or interaction between iron and chromium particles (Fig. 2b) and these results are consistent with XRD data. In the case of the chromium modified samples, the band at about 250, 350 and 450 nm are connected with the presence of tetrahedrally coordinated Cr^{6+} into small mono- or polychromate species [32]. The slight absorption above 600 nm is assigned to the presence of Cr^{3+} in ion-exchange positions ($Cr^{3+}\rightarrow Cr^{6+}$) or in Cr_2O_3 or Cr_xO_y clusters [32]. In accordance with XRD and FTIR data, the observed changes in absorption above 350 nm for all bi-component materials confirm the assumption done above for the existence of strong interaction between metal ions and/or to the improved metal oxides dispersion.

Mossbauer spectroscopy was applied to obtain more information about the phase composition, cationic occupations and/or different state distribution of iron ions in the studied oxide materials (Table 1). The characteristic parameter, isomer shift (IS), quadruple splitting (QS) and the relative part of each component (G) are listed in Table 1. The spectra of all oxide materials consist of doublet components. Their parameters indicate presence of paramagnetic or super paramagnetic phases, where iron is in trivalent state and octahedral coordination. The relatively high values of quadrupole splitting (QS), could be due to the spinel lattice distortion caused by the formation of oxygen vacancies. The QS parameters increase with the increase of chromium content in the samples (Table 1). This evidences that with the increase of chromium content in the samples the electric field around the iron cores becomes more asymmetric. This confirms the presence of chromium in the vicinity of the iron in proportion to the chromium content in the sample.

Table 1. Moessbauer parameters for all iron and chromium oxide materials.

Sample	**Components**	**IS, mm/s**	**QS, mm/s**	**G_{exp}, mm/s**
Fe/SiO_2	Db - Fe^{3+}_{octa}	0.34	0.77	0.52
$2Fe1Cr/SiO_2$	Db - Fe^{3+}_{octa}	0.33	0.87	0.52
$1Fe1Cr/SiO_2$	Db - Fe^{3+}_{octa}	0.33	0.93	0.54
$1Fe2Cr/SiO_2$	Db - Fe^{3+}_{octa}	0.31	1.03	0.68

To study changes in catalysts reducibility, iron and chromium materials were analyzed by TPR (Fig. 3). TPR profile of Fe/SiO_2 shows one reduction peak at about 630 K. According to the UV-Vis and Mossbauer data, this effect belongs to the reduction of Fe_2O_3 to Fe_3O_4 [32]. The second peak above 670 K originates with partial two step reduction of Fe_3O_4 to FeO and FeO to metallic Fe [19, 32-35]. The TPR effects for the binary oxide materials were broader and shifted to higher temperature as compared to the corresponding individual iron modification. This evidence change in the environment of iron ions, most probably due to the formation of ferrite phase (Table 1) [29, 36, 37]. The complexity of the TPR profile of $2Fe1Cr/SiO_2$ can tentatively attributed to the existence of hematite and magnetite impurities in the spinel phase (Fig. 3).

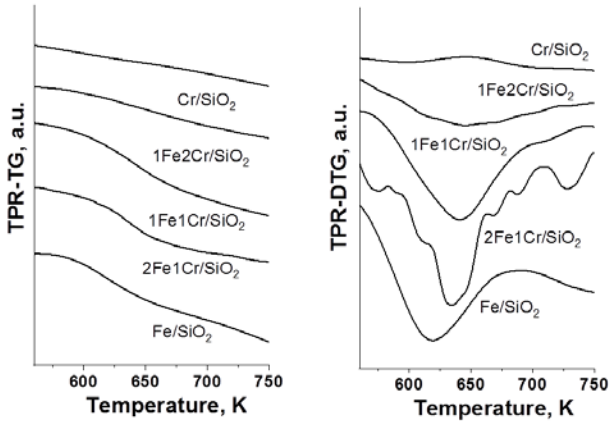

Fig. 3. TPR-TG and TPR-DTG profiles for all iron and chromium oxide materials.

In Fig. 4 are demonstrated the temperature dependencies of methanol decomposition on various iron and chromium modifications. The conversion is observed above 650 K and CO, methane, dimethyl ether (DME) and CO_2 in different proportions are detected.

Among the mono-component materials, the pure iron oxide demonstrates higher catalytic activity in methanol decomposition to syngas. The appearance of a plateau in its conversion curve above 680K is evidence for catalyst deactivation. In accordance with the TPR data (Fig. 3) this could be assigned to reduction transformations with the active magnetite phase. The observed high selectivity to methane (at 30% concession, 98% for Fe/SiO_2, 67% for $2Fe1Cr/SiO_2$, 43% for $1Fe1Cr/SiO_2$ and 50% for $1Fe2Cr/SiO_2$) could be related to facile C-O bond scission in the adsorbed methanol molecules due to the simultaneous activity of strong basic (oxygen ions) and acid (iron ions) sites in magnetite and/or hematite species. The Cr/SiO_2 material exhibits extremely low catalytic activity during the whole temperature interval and maximum conversion of about 40% is detected just at 700 K. At this temperature a fast decrease in the conversion is observed (Fig. 4), most probably due to the aggregation of the active phase and/or formation of non-desorbable products.

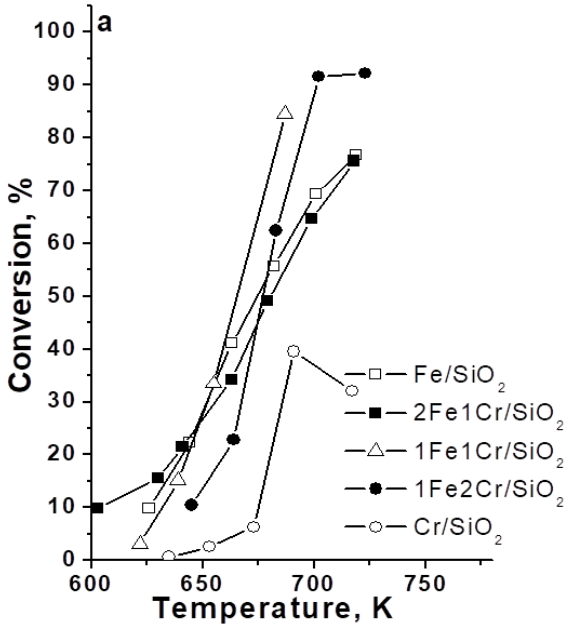

Fig. 4. Methanol conversion for all iron and chromium oxide materials.

All binary materials exhibit improved catalytic behavior as compared to the individual oxides (Fig. 4). The extremely high activity is observed for the sample with equimolar Fe/Cr ratio ($1Fe1Cr/SiO_2$) which could be due to the formation of finely dispersed spinel phase (Fig. 1, Table 1). The impact of the activity of Cr^{3+}-Fe^{2+} redox pairs, situated in the highly exposed to the reactants octahedral positions in the spinel lattice could be proposed. In accordance with the TPR data, the lowest catalytic activity for the binary material with the highest Fe/Cr ratio could be attributed to the existence of FeO_x impurities in the spinel phase. The stability of all catalysts was examined after the catalytic test up to 773 K. All oxide materials retain their catalytic activity and selectivity, with the exception of mono-component chromium oxide, in which low stability is observed. A common feature of the binary catalysts is their improved stability to the influence of the reaction medium. This could be due to the fast release of the formed during the reaction carbon deposits *via* oxidation from the high mobile oxygen ions from the spinel lattice.

CONCLUSION

Supported on silica nanosized iron and chromium spinel oxides could be successfully synthesized using wet impregnation technique with aqueous solutions of metal salts in appropriate ratio. Their composition could be tuned with the Fe/Ce ratio. The equimolar Fe/Cr content facilitates formation of more homogeneous and finely dispersed materials. They demonstrate extremely high catalytic activity and improved stability in methanol decomposition in a wide temperature interval.

Acknowledgements: *This work was supported by the Bulgarian Ministry of Education and Science under the National Research Programme "Young scientists and postdoctoral students" approved by DCM#577/17.08.2018 and the Bulgarian Science Fund Contract No КП-06-Н29/2. Project BG05M2OP001-1.002-0019: „Clean technologies for sustainable environment – water, waste, energy for circular economy"(Clean&Circle), for development of a Centre of Competence is also acknowledged.*

REFERENCES

1. T. Rauckyte, D. J. Hargreaves, Z. Pawlak, *Fuel*, **85**, 481 (2006).
2. A. Pohar, D. Belavi, G. Dolan, S. Hocevar, *J. Power Sources*, **256**, 80 (2014).
3. S. T. Yong, C. W. Ooi, S. P. Chai, X. S. Wu, *Inter. J. Hydrogen energy*, **38**, 9541 (2013).
4. A. Qi, B. Peppley, K. Karan, *Fuel Process. Technol.*, **88**, 3 (2007).
5. M. Luo, Y. Yi, S. Wang, Z. Wang, M. Du, J. Pan, Q. Wang, *Renew. Sustain. Energy Rev.*, **81**, 3186 (2018).
6. J. Rifkin, The Hydrogen Economy, Penguin Publishing Group, 2003.
7. L. Chmielarz, M. Jabłońska, *RSC Adv.*, **5**, 43408 (2015).
8. P. Li, R. Zhang, N. Liu, S. Royer, *Appl. Catal., B*, **203**, 174 (2017).
9. L. Chmielarz, A. Węgrzyn, M. Wojciechowska, S. Witkowski, M. Michalik, *Catal. Lett.*, **141**, 1345 (2011).
10. M. Jabłońska, A. Król, E. Kukulska-Zając, K. Tarach, L. Chmielarz, K. Góra-Marek, *J. Catal.*, **316**, 36 (2014).
11. R. Prasad, G. Rattan, *Bull. Chem. React. Eng. Catal.*, **5**, 7 (2010).
12. L. Chmielarz, M. Jabłońska, A. Strumiński, Z. Piwowarska, A. Węgrzyn, S. Witkowski, M. Michalik, *Appl. Catal. B*, **130–131**, 152 (2013).
13. J. Pinkas, V. Reichlova, R. Zboril, Z. Moravec, P. Bezdicka, J. Matejkova, *Ultrason. Sonochem.*, **15**, 257 (2008).
14. X. Liao, J. Zhu, W. Zhong, H.-Y. Chen, *Mater. Lett.*, **50**, 341 (2001).
15. X. Liu, K. Shen, Y. Wang, Y. Wang, Y. Guo, Y. Guo, Z. Yong, G. Lu, *Catal. Commun.*, **9**, 2316 (2008).
16. J. Boon, E. van Dijk, Ö. Pirgon-Galin, W. Haije, R. van den Brink, *Catal. Lett.*, **131**, 406 (2009).
17. A. Sun, Z. Qin, S. Chen, J. Wang, *Catal. Today*, **93–95**, 273 (2014).
18. Y. K. Shin, H. Kwak, A. V. Vasenkov, D. Sengupta, A. C. T. van Duin, *ACS Catal.*, **5**, 7226 (2015).
19. M. García-Vázquez, K. Wang, J. M. González-Carballo, D. Brown, P. Landon, R. Tooze, F. R. García-García, *Appl. Catal. B: Environmental*, **277**, 119139 (2020).
20. V. S. Jaswal, A. K. Arora, M. Kinger, V. dev Gupta, J. Singh, *Oriental J. Chem*, **30**, 559 (2014).
21. C. Martos, J. Dufour, A. Ruiz, Inter. *J. Hydrogen Energy*, **34**, 4475 (2009).
22. M. Selvarej, A. Pandurangan, K.S. Seshadri, *Appl. Catal. A: Gen.*, **242**, 347 (2003).
23. D. S. Nair, Manju Kurian, J. *Hazardous Mater.*, **344**, 925 (2018).
24. J. C. Gonzalez, M. G Gonzalez, M. A Laborde, N. Moreno, *Appl. Catal.*, **20**, 3 (1986).
25. S. Musić, S. Popović, M. Ristić, *J. Mater. Sci.*, **28**, 632 (1993).
26. T. Ramachandran, F. Hamed, *Mater. Res. Bull.*, **95**, 104 (2017).
27. J. E. Amonette, D. Rai, *Clays Clay Miner.*, **38**, 129 (1990).
28. R. K. Sharma, R. Ghose, *Ceram. Inter*, **41**, 14684 (2015).
29. S. Zheng, L. Gao, J. Gao, *Mater. Chem. Phys.*, **71**, 174 (2001).
30. A. Wang, Y. Wang, E. D. Walter, R. K. Kukkadapu, Y. Guo, G. Lu, R. S. Weber, Y. Wang, C. H. F. Peden, F. Gao, *J. Catal.*, **358**, 199 (2018).
31. Y. Xia, W. Zhan, Y. Guo, Y. Guo, G. Lu, *Chin. J. Catal.*, **37**, 2069 (2016).
32. Y. Cheng, F. Zhang, Y. Zhang, C. Miao, W. Hua, Y. Yue, Z. Gao, *Chin. J. Catal.*, **36**, 1242 (2015).
33. F. Ayari, M. Mhamdi, T. Hammedi, J. Álvarez-Rodríguez, A. R. Guerrero-Ruiz, G. Delahay, A. Ghorbel, *Appl. Catal. A Gen.*, **439–440**, 88 (2012).
34. A. Pineau, N. Kanari, I. Gaballah, Thermochim., *Acta*, **447**, 89 (2006).
35. R. Köhn, D. Paneva, M. Dimitrov, T. Tsoncheva, I. Mitov, C. Minchev, M. Fröba, *Microporous Mesoporous Mater.*, **63**, 152 (2003).
36. S.S. Reddy Putluru, A. D. Jensen, A. Riisager, R. Fehrmann, *Top. Catal.*, **54**, 1286 (2011).
37. L. Li, Q. Shen, J. Li, Z. Hao, Z. Ping Xu, G.Q.M. Lu, *Appl. Catal. A Gen.*, **344**, 131 (2008).